Engineering light absorption in single-nanowire solar cells with metal nanoparticles

2011 New J. Phys. 13 123026

(http://iopscience.iop.org/1367-2630/13/12/123026)

New Journal of Physics
The open-access journal for physics

Engineering light absorption in single-nanowire solar cells with metal nanoparticles

Carlo Colombo[1], Peter Krogstrup[2], Jesper Nygård[2], Mark L Brongersma[3] and Anna Fontcuberta i Morral[1,4]

[1] Laboratoire des Matériaux Semiconducteurs, Ecole Polytechnique Fédérale de Lausanne, 1015 Lausanne, Switzerland
[2] Nano-Science Center, Niels Bohr Institute, University of Copenhagen, Denmark
[3] Geballe Laboratory of Advanced Materials, Stanford University, CA 94305, USA
E-mail: anna.fontcuberta-morral@epfl.ch

New Journal of Physics **13** (2011) 123026 (14pp)
Received 20 September 2011
Published 16 December 2011
Online at http://www.njp.org/
doi:10.1088/1367-2630/13/12/123026

Abstract. Semiconductor nanowires (NWs) possess a fascinating ability to efficiently collect and trap light into a sub-wavelength volume due to the occurrence of leaky mode resonances. The same confinement ability is manifested by metal nanostructures thanks to the excitation of surface plasmons. Combining the two systems, we show how light absorption in individual NWs can be spectrally tailored and enhanced by decorating them with metal nanoparticles. This is demonstrated by means of scanning photocurrent measurements on individual NWs and interpreted by full-field simulations.

S Online supplementary data available from stacks.iop.org/NJP/13/123026/mmedia

[4] Author to whom any correspondence should be addressed.

Contents

1. Introduction

The optical properties of semiconductor nanowires (NWs) and microwires are currently the focus of attention because of their potential applications in a variety of opto-electronic devices [1–3], such as the photovoltaic [4–6], photo-detectors [7], optical switches [8], antennas [9, 10], meta-materials [11–13] and thermal emitters [14]. The possibility of manipulating light interaction with nanoscale objects has fascinated the whole nanoscience and nanotechnology community. For example, it has recently been shown that the spectral dependence of light absorption in an NW can be strongly influenced by its diameter [15, 16]. This is related to resonant optical phenomena that were predicted by Mie in the case of spherical particles in 1908 [17]. The high-refractive-index NW forms a cavity in which light can circulate by multiple total internal reflections from the boundaries often referred to as leaky mode resonances (LMRs) [18]. The same ability to confine and trap light in a deep sub-wavelength region is shared by metal nanostructures thanks to the excitation of collective electron oscillations known as surface plasmons (SPs) [19]. Plasmon-driven light enhancement effects can lead to a substantial increase in the local density of optical states, which is exploited to boost light absorption in solar cells [20–22] and detectors as well as luminescence [23]. Additionally, the coupling of plasmon resonances with organic and inorganic materials has been used to increase the Raman tensor by several orders of magnitude (surface-enhanced Raman scattering). This has enabled single-molecule detection and opened a new field of research [24]. A hybrid system formed by semiconductor NWs and metal nanoparticles implies the additional possibility of light absorption by the coupling of plasmon excitations in the metal with the absorption resonances of the NW. Recently, it has been shown that this system can result in the local enhancement of photocurrent of very-small-diameter NWs [25].

The scope of this paper is to study how NW leaky modes can be modified by interaction with metal particles in a general way. In the case of NWs decorated with metallic particles, we show how the symmetry of the wire and the particle modes plays a critical role in the optical interaction between these objects. For this reason, each NW mode is affected in a different way, with the generation of an enhancement, suppression or shift in the resonant position and intensity. More specifically, we conduct studies on a single GaAs core-shell p–i–n junction. This allows for a direct comparison to full-field simulations without the challenges involved in ensemble averaged measurements. The results are also directly applicable to real NW-based photovoltaic devices and detectors. Spectral photocurrent measurements on bare NWs and with the presence of metal particles on the top or side facets are carried out and analyzed in detail with full-field simulations.

This paper is divided into three parts. In the first, the details of the growth of NWs, along with the procedure for sample preparation, are given. In the second, the light absorption properties of bare NWs are discussed and explained considering the interference with the cavity created in the underlying SiO_2 layer. Using the knowledge developed for bare NWs, it is finally possible in the third part of the paper to analyze the effect of the metal particles. The effect of their exact location on the NW surface is investigated in great detail and, using simulation, we demonstrate that it is critical to control the spacing between the metal particle and the NW to obtain large absorption enhancements.

2. Sample preparation and experimental methods

Thanks to advances in the understanding of growth mechanisms [26–31], NWs can now be obtained in a variety of materials with excellent control of the morphology, doping concentration and crystal structure. This has led to the possibility of studying novel fundamental phenomena and to the reliable fabrication of NW-based devices [32–34]. Among the devices are radial p–n junctions, which are believed to play a role in third-generation solar cells [35]. Recently, we showed that self-catalyzed growth of NWs with molecular beam epitaxy (MBE) can be obtained with extremely homogeneous core-shell hetero-structures and with excellent optical properties [36, 37]. We have also demonstrated the fabrication of highly efficient p–i–n junctions [38]. As will be shown in the following, the control of homogeneity in the diameter and core-shell structures is an essential part of this study that otherwise could not be conducted.

The GaAs p–i–n NWs are grown on a silicon substrate by the MBE method. The core is obtained via a self-catalyzed vapor liquid solid process [30], with a nominal Ga growth rate of $0.27\,\mu m\,h^{-1}$, for 45 min, at $T = 630\,^{\circ}C$ and a V/III ratio of 60. The p-doping is achieved with a beryllium flux corresponding to a doping level of 3.5×10^{19} atoms cm^{-3} for planar growth. The diameter of the core is about 120 nm. After the growth of the doped core, the MBE conditions are switched from axial to radial growth: the substrate temperature is lowered down to $460\,^{\circ}C$, the As source is switched from As_4 to As_2 and the V/III ratio is increased to 150 [39, 40]. After the growth of 30 nm without any intentional impurity to create an intrinsic layer, a 60 nm n-doped shell is grown, using silicon as a dopant, with a nominal concentration of 5×10^{18} atoms cm^{-3}. The overall diameter of the final structure is about 300 nm, while the length is approximately $10\,\mu m$.

The devices were prepared by transferring NWs to an oxidized Si substrate with $1\,\mu m$ layer of SiO_2. The electrical contacts to the p and n parts were realized in a double-step electron beam lithography (EBL) procedure. Ag nanoparticles with ~100 nm diameter were also defined by EBL. A thin layer of 7 nm of SiO_2 was evaporated between the NW and the metal particles in order to avoid damping of the SP resonance by the absorbing semiconductor [41], thereby maximizing the optical interaction between the metal particle and the NW. An illustration of the final device is presented in figure 1(a). The different colors of the NW represent the different dopings: green for the n-shell and red for the p-core. A scanning electron microscopy (SEM) image of the nanoparticles deposited on the NW is shown in the inset of figure 1(a), while a typical device is shown in figure 1(b).

The absorption properties of the NWs were investigated experimentally by scanning photocurrent measurements. A laser focused to a spot of about $1.5\,\mu m$ was scanned across the device and the short circuit current produced was acquired at each position. The excitation

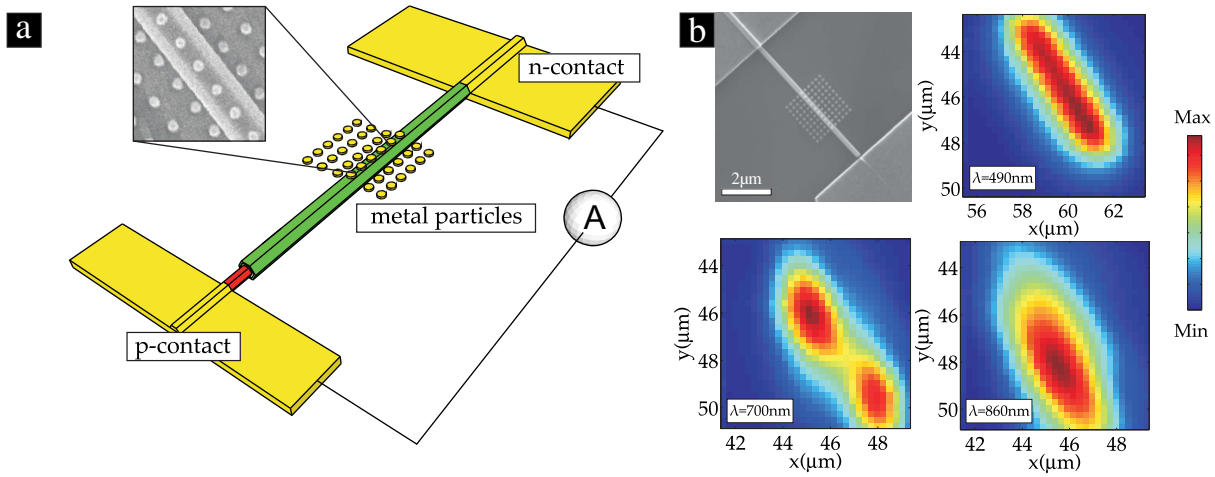

Figure 1. (a) Illustration of a contacted radial p–i–n junction GaAs NW. The different colors of the NW represent the regions with the different doping, green for the n-shell and red for the p-core. An array of metal particles is deposited on top of the NW. A current meter is connected in series to measure the short circuit current produced when a focused laser beam is scanned over the structure. The inset shows an SEM image of the array of particles deposited on the NW. (b) An SEM image of a typical device is shown in the top left corner of the picture. The other images show examples of photocurrent maps (x and y are spatial coordinates while the color map represents the intensity of the measured short circuit current) with all the possible effects induced by the metal particles: absorption suppression at $\lambda = 700$ nm, enhancement at $\lambda = 860$ and no effect at $\lambda = 490$ nm.

source was a white light super-continuum source (Fianium) coupled to an acousto-optic tunable filter. The incoming wavelength was tuned from 480 to 880 nm with steps of 10 nm. Top-illuminated, bare NWs can exhibit enhanced absorption due to the excitation of transverse electric (TE) LMRs with the electric field normal to the wire axis and transverse magnetic (TM) LMRs with the magnetic field normal to the wire axis. When the diameter of the NW is larger than 200 nm the light absorption enhancement in TE or TM polarization is of similar magnitude and nature. For this reason, in this paper we focus only on the TE polarization case. Our devices consist of a contacted p–i–n junction with a 2 μm long array of nanoparticles in the middle. The current–voltage characteristic curve of these devices exhibits rectifying behavior, as shown in the supplementary material (available from stacks.iop.org/NJP/13/123026/mmedia). The distance between the contacts is about 7 μm. This leaves enough space between the nanoparticle array and the contacts, so that we can distinguish the photocurrent response between regions with and without particles. Typical photocurrent maps of a device at different wavelengths are shown in figure 1(b). For certain wavelengths such as 860 nm, the metal particles induce an increase in the NW light absorption. For other wavelengths such as 700 nm the presence of nanoparticles reduces the absorption in the NW or no observable changes can be detected (490 nm).

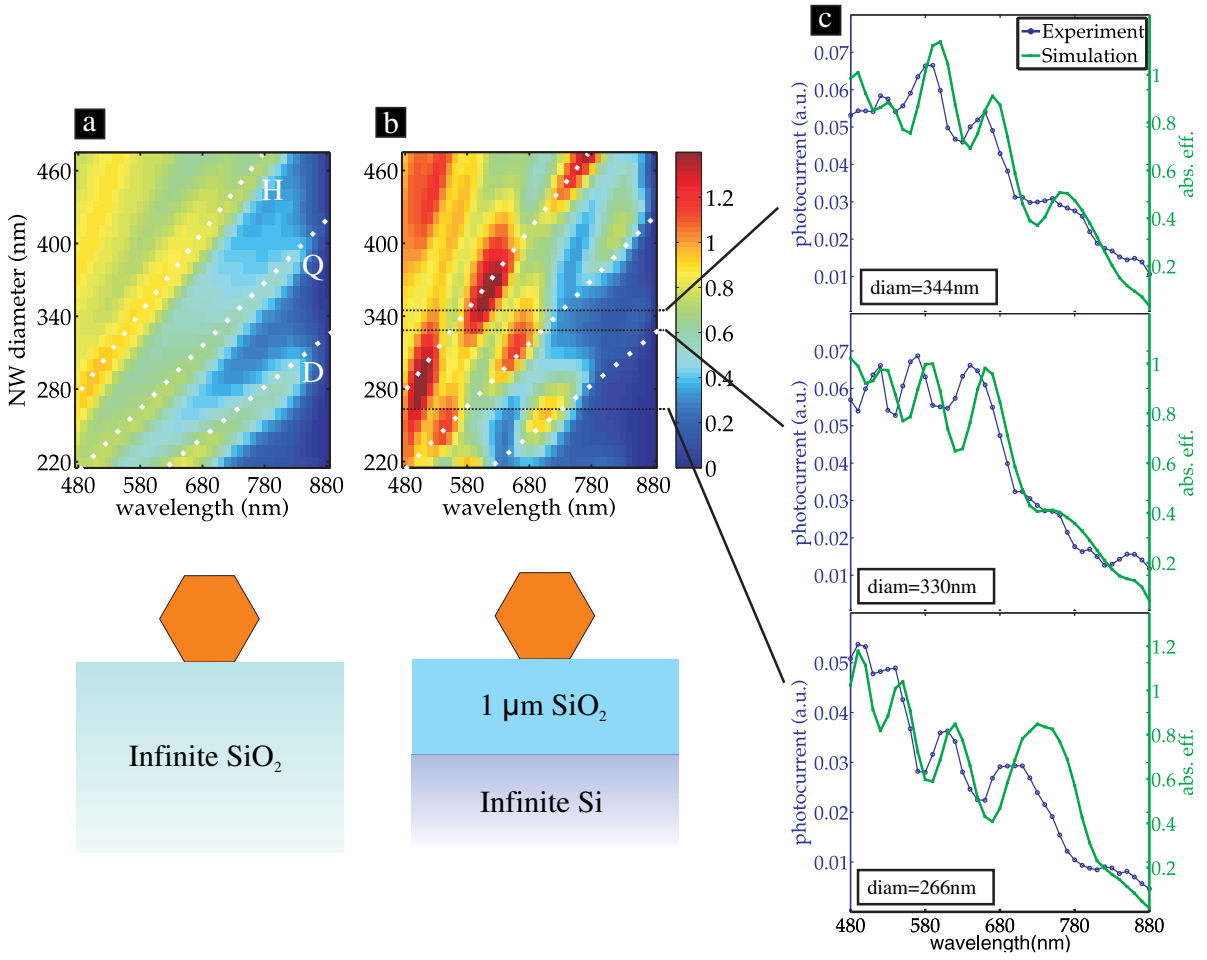

Figure 2. (a) Calculated absorption efficiency map for an NW lying on a semi-infinite SiO_2 substrate as a function of the radius and excitation wavelength. The dashed lines are used as a guide to the eye in the identification of the leaky mode resonances. (b) The same calculation in the case of a substrate consisting of 1 μm of SiO_2 and a semi-infinite Si substrate. (c) Comparison between experimental photocurrent measurements and absorption efficiency simulations for nanowires with different diameters: 344, 330 and 266 nm.

3. Optical absorption of bare nanowires (NWs)

We start by studying the optical absorption properties of the bare NWs (without the metal nanoparticles). As mentioned above, the absorption of light in a single NW is governed by the existence of LMRs [15, 42] in which the NW is treated as a sub-wavelength resonator. Assuming an infinitely long cylinder, the excitation of leaky modes can be predicted analytically as a function of the dielectric constant and wire diameter by analytically solving Maxwell's equations with appropriate boundary conditions. The same modes in NWs of a more complex cross section can also be computed using a full-field finite-difference frequency-domain (FDFD) simulation [43]. Using this approach, the exact hexagonal geometry of the NW can be precisely considered. Figure 2(a) shows FDFD-simulated absorption efficiency (AE) maps as a function

of wavelength for NWs with a diameter in the same range as those used in the experiments, sitting on a semi-infinite SiO_2 substrate.

We define the AE as the ratio between the energy flux absorbed in the NW and the energy flux impinging the projected area of the NW, which is equal to the ratio of the absorption and geometrical cross sections of the NW. The magnitude of the AE may exceed 1 if the wavelength and NW diameter match a strong resonance mode and the NW effectively performs an antenna function. Since the circumference of the NWs used in this study is relatively large compared to the excitation wavelength in the high-index semiconductor, several high-order modes are supported. The dashed white lines in the picture refer to the occurrence of resonant modes. The labels D, Q and H are used to name the resonances involved; they stand, respectively, for dipole, quadruple and hexapole, from the number and symmetry of the maxima of the electromagnetic field involved in the resonance. The physical meaning of this nomenclature will be used in the rest of the paper and will be clearer in the next section. A two-dimensional plot of the calculated AE as a function of the wavelength and diameter of the NW for the substrate geometry used in the experiment is shown in figure 2(b). The substrate consists of an oxidized Si wafer with a 1 μm thick SiO_2 layer. In our analysis of the NW photocurrent spectra, it is important to point out that the substrate can play an important role and that the absorption in the wire oscillates as a function of the SiO_2 layer thickness. In fact, the NW is now part of a low-quality-factor Fabry–Pérot cavity for which two mirrors correspond to the interface with the high-refractive-index Si substrate and the NW itself. The interference between the Fabry–Pérot and the NW resonances gives rise to the strong modulation in the AE seen in figure 2(b). Interestingly, the coupling between the two cavities can give rise to an increase in the NW AE up to 50% with respect to an NW embedded in a constant dielectric environment (e.g. in a matrix or suspended in air).

Next, we relate the calculated spectral dependence of the AE to the measured photocurrent spectra. It is possible to relate these two quantities directly by assuming that the internal quantum efficiency is wavelength and spatially independent. For this to be realistic the extension of the depletion region should cover most of the NW cross section and the thermalization of carriers should occur at a much higher rate than the carrier recombination. The results obtained for three NWs with diameters of 266, 330 and 344 nm are presented in figure 2(c). The blue curves indicate the photocurrent measurements renormalized to the incoming photon flux, while the green ones show the calculated AEs. In all cases, the photocurrent tends to decrease when the wavelength is increased towards the GaAs bandgap (872 nm at room temperature). As expected from the calculations reported before, we observe several oscillations in the photocurrent that are related to the interplay between the NW resonances and the underlying SiO_2 cavity. For all three NW diameters the experimental curve is in quite good agreement with the calculated AE.

4. Optical absorption of NWs decorated with metal particles

Having shown the absorption properties of the bare NWs and the important role of the substrate, we move forward to investigate the interaction of the wire with the silver nanoparticles. In figure 3(a), we show the AE map of an NW with a silver particle located on the top facet, as a function of NW diameter and excitation wavelength. The simulation is performed considering an infinite SiO_2 substrate in order to highlight the effect of the metal particles and to decouple it from the interference generated by the substrate. A complete simulation

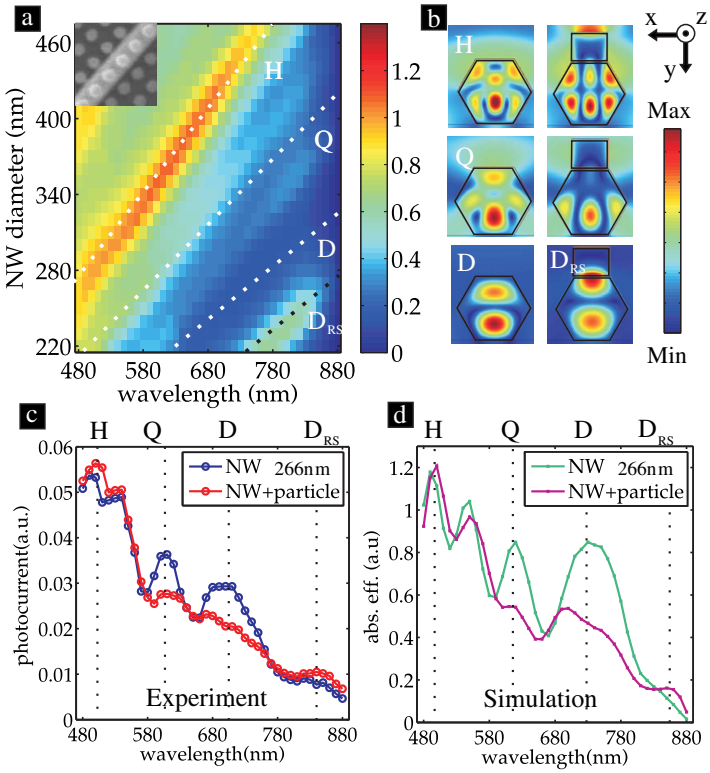

Figure 3. (a) Simulation of the absorption efficiency for an NW with metal particles deposited *on the top* facet with respect to the nanowire radius and wavelength. The different letters label the resonant modes of the nanowire: H—hexapole, Q—quadrupole, D—dipole, D_{RS}—dipole red shifted. (b) Plots of the absolute value of the magnetic field in the z-direction. The left column shows the field patterns in a 266 nm diameter NW obtained without metal particles for the different resonant modes while in the right one the modification of these patterns by the metal particle is reported. The color scale used is the same for the picture in the left and in the right column. (c) Photocurrent as a function of the incoming wavelength for a bare nanowire with a diameter of 266 nm (blue) and for a nanowire with a particle (red). (d) Simulation of absorption efficiency for the same nanowire diameter with (light blue) and without (magenta) metal particles.

considering the sum of the two interactions is reported in the supplementary material (available from stacks.iop.org/NJP/13/123026/mmedia).

Similarly to the bare NW case, we observe that the existence of LMRs dominates the features of the absorption spectrum. For an easier comparison, we indicate the spectral position of the resonances for the case of the bare NWs (white dashed lines). Counter-intuitively, the presence of the metal particles results in a change in the intensity and a shift of the LMRs. Interestingly, each of the LMRs is perturbed in a different way. In order to understand this, one needs to consider the nature of each of the LMRs. The first one (D) shifts to longer wavelengths (D_{RS}), the second one (Q) disappears and the third one (H) becomes more intense.

The modification induced by the particles depends only on the symmetry of the mode that it couples to and only indirectly on the wavelength and diameter at which the mode occurs.

We now turn our attention to understanding how the spectral dependence of the photocurrent generation can be tailored and enhanced by engineering the coupling of the NW modes and plasmonic modes of the metal particles. To this end, it is important to understand the field distribution inside the semiconductor NW, where absorption and electron–hole pair generation take place. The field distribution in the NW is related to the modal interaction of the NW modes and plasmonic modes of the particle. The nature and strength of this interaction are related to the field distributions and the symmetry of the relevant interacting modes. At different excitation frequencies different modes in the NW and metal particles are excited and different interactions can be expected.

Maps of the field patterns obtained under resonant excitation of modes with D, Q and H symmetry in a 266 nm diameter NW are reported in the left column of figure 3(b). The field maps in the right column of figure 3(b) show how these field distributions are modified due to the presence of a metallic nanoparticle. The spatial distribution of this field component most clearly visualizes the multipolar symmetry of the NW and best highlights the presence of SPs.

We will use these maps to explain the trends in the experimentally observed photocurrent measurements (figure 3(c)) and corresponding simulated absorption spectra. To facilitate a simple analysis, we have indicated the different multipolar resonances with vertical dashed lines. Comparing the last two figures, one can see that not only is the qualitative behavior of the modes well described by the simulations, but also the relative intensity of the variations is in excellent agreement.

As we increase the illumination wavelength, we can see in the field plots and spectra that we can sequentially excite hexapolar (H), quadrupolar (Q) and ultimately dipolar (D) resonances. Just as the field distribution in the NW changes with increasing wavelength, the SP-related fields around the metallic nanoparticle evolve as well. At short wavelengths where the H mode of the NW is excited (top field map), a high magnetic field intensity can be observed across the top of the metallic particle. In general, the presence of high magnetic fields right at a metal/air interface that decays rapidly away into the metal and dielectric is characteristic of an SP excitation. These magnetic fields are related to the collective electron current oscillations (SP) via Ampere's law. The presence of a single maximum on the top of the metallic nanoparticle indicates a lowest-order SP resonance with roughly half of an SP wavelength, $\lambda_{sp}/2$, fitting across the top width of the particle [44]. A higher order ($3\lambda_{sp}/2$) resonance weakly excited (slightly off resonance) appears at the interface between the metal particle and high-index GaAs NW. The excitation of this latter SP resonance provides minor enhancement in the fields in the NW and thus gives rise to a relatively small but measurable boost in the light absorption/photocurrent in both the experiment (figure 3(c)) and simulation (figure 3(d)). As the wavelength is increased, the NW first exhibits a Q resonance. The absence of a resonance in the metal particle in this frequency range results in an overall suppression of the fields in the NW and a reduction in the photocurrent. It can be seen that the presence of the nanoparticle effectively suppresses one of the modal field maxima in the wire. Near the D resonance frequency of the wire, there is a significant boost in the measured photocurrent (up to a factor 1.5) and simulated absorption (up to a factor 2.5). At this long wavelength, one effectively drives a strong $\lambda_{sp}/2$ SP mode at the interface between the metal particle and the NW, which enhances the fields inside the wire. As a consequence, there is a spatial shift of one of the two poles of the mode toward the metal that is required to ensure maximum magnetic field intensity at the metal semiconductor boundary

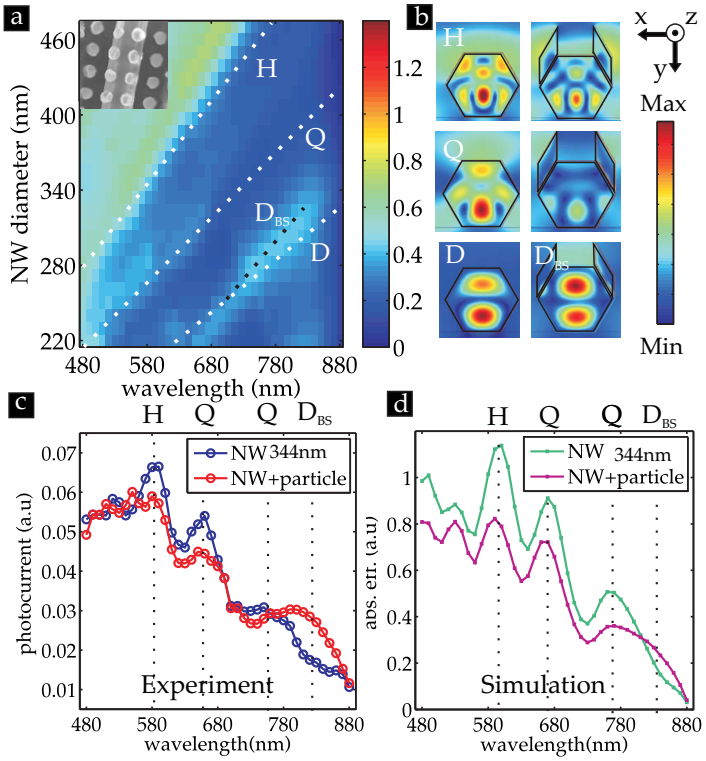

Figure 4. (a) Simulation of the absorption efficiency for an NW with metal particles deposited *on the side* facets with respect to the nanowire radius and wavelength. The different letters name the resonant modes of the nanowire: H—hexapole, Q—quadrupole, D—dipole, D_{BS}—dipole red shifted. (b) Plots of the absolute value of the magnetic field in the z-direction. The left column shows the field profiles obtained without metal particles for the different resonant modes while the right column shows the modification of the mode by the metal particle. The color scale used is the same for picture in the left and in the right column. (c) Photocurrent as a function of the incoming wavelength for a bare nanowire with a diameter of 344 nm (blue) and for a nanowire with a particle (red). (d) Simulation of absorption efficiency for the same nanowire diameter with (light blue) and without (magenta) metal particles.

(characteristic of the SP excitation). Effectively, this makes the wire appear slightly larger and intuitively the resonance should shift to longer wavelengths. Such a red shift in the dipolar resonance of the individual wire to a metal decorated wire is indeed observed going from D to D_{RS}.

We now turn to the role of the nanoparticles' exact location on the NW facets. We have seen how the presence of the surface plasmon polaritons (SPPs) on the NW top facet changes the field distribution of the modes. It is therefore reasonable to expect that changing the position of the metal nanoparticles will give rise to different interactions between NW and SP fields. This constitutes a further handle on the engineering of light absorption in the NWs. We have performed the FDFD AE calculations and spectral photoconductivity experiments (figure 4) in NWs having nanoparticles sitting on the *top side* facets, as shown in the inset of figure 4(a) and simulations shown in the right column in figure 4(b). In this case the simulated absorption

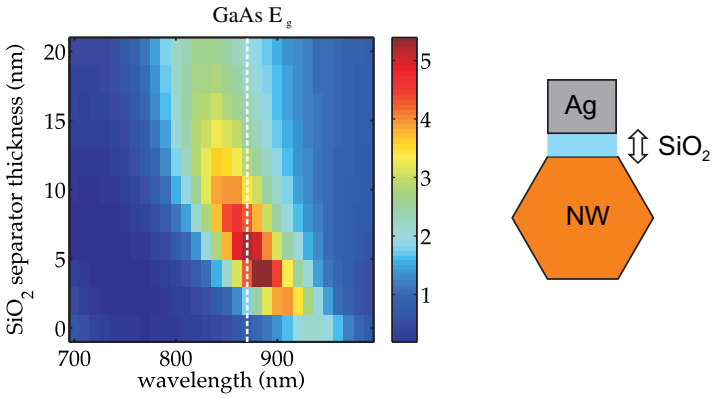

Figure 5. Simulation of the ratio of absorption efficiency between the nanowire with particles and the bare nanowire, as a function of thickness of the SiO_2 separator layer and wavelength. The dashed white line represents the energy position of the GaAs band gap.

spectra also exhibit good overall agreement with the experimental data collected with an NW of 344 nm diameter (figures 4(c) and (d)). The fact that two quadrupole-like modes appear is the consequence of the mode interference with the silicon dioxide cavity below the NW, which gives rise to a modulation of the resonance.

As expected, the interaction generates a different effect on the AE spectrum. In this case both the hexapole- and quadrupole-like modes of the wire undergo a strong suppression. The field distributions show that SPs are primarily excited on the metal/air interfaces, where they do not contribute to the absorption in the NW and thus the photocurrent. Near the dipolar resonance, an SP resonance [44] is excited for which approximately a full λ_{sp} fits along the interface between the NW and metal particle. Driving that resonance can enhance the photocurrent at the long wavelength side of the spectrum and thus increase the operational bandwidth of GaAs-based NW photo-detectors.

Finally, we predict that light absorption can be manipulated even further by varying one more key geometrical parameter: the thickness of the SiO_2 spacer between the NW and the metal nanoparticles. Here, we focus our attention on the region around the band gap for two reasons: (i) the optical absorption here is intrinsically low; (ii) it is the relevant energy region for optical interconnections, where the emitter and the detector should be in the same spectral region. We have analyzed in more detail the dipole-like resonance in the case of metal particles sitting on the NW top facet. Figure 5 shows the ratio between AEs with and without the metal particles as a function of spacer thickness and wavelength, for an NW with a diameter of 250 nm.

The resonance peak can be tuned over about 80 nm by varying the separator thickness between 0 and 10 nm. The peak position is determined by the SPP frequency, which is a consequence of fulfilling a resonance condition for the SPs traveling back and forth between the two extremities of the metal particle [44]. The high tunability of the resonance position as a function of the oxide thickness is a consequence of the large variation of the refractive index experienced by the SP mode when the spacer thickness is varied. For small enough thicknesses, the SP mode overlaps partially with the low-index oxide and partially with the high-index semiconductor NW. When the oxide layer is thickened, the effective mode index of the SP decreases, with a consequent increase of the SP wavelength. As a consequence, the resonant

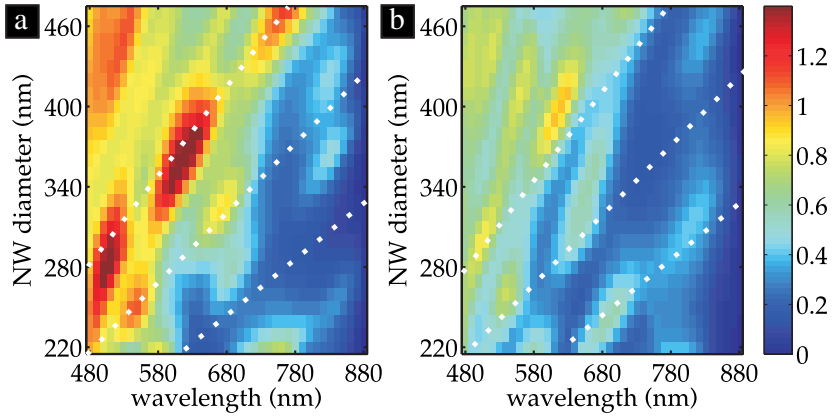

Figure 6. (a) Simulation of the absorption efficiency for an NW with metal particles deposited *on the top* facet with respect to the nanowire radius and wavelength. Differently from figure 3(a), the simulation is performed considering the real substrate consisting of a Si substrate coated with 1 μm SiO_2. (b) The same simulation calculated for particles located *on the side* facets. The white-dashed lines are used to indicate the position of the resonant modes for bare NWs lying on a semi-infinite SiO_2 substrate.

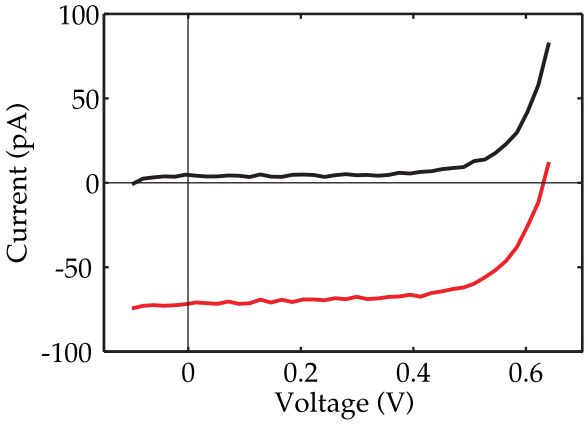

Figure 7. Typical I–V curve of an NW solar cell, showing the rectifying behavior, in the dark (black curve) and under an illumination of 1 sun (red curve).

condition is met for shorter wavelengths and a blue shift of the resonance in the absorption occurs. Additionally, we find that by choosing the SiO_2 thickness appropriately, the AE at the band gap can be increased up to five times. The fact that the highest absorption in the NW occurs for a few nanometers spacing and not at zero spacing may seem counter-intuitive. However, it is now well established from research on plasmon-enhanced photovoltaics that particles need to be spaced by a few nanometers from an absorbing semiconductor to avoid significant damping of the SP resonance [41] (figures 6 and 7).

5. Conclusion

In conclusion, we demonstrate how light absorption in NWs through the LMRs can be further engineered by choosing the appropriate geometry of the substrate and the interaction with SP modes on the particles. We demonstrate this for NWs with relatively large diameters, where the leaky modes were expected to play a less significant role (about 300 nm). The interaction of the leaky modes with the substrate is shown to generate a modulation effect on each resonant mode: the light absorption intensity of each leaky mode changes in an oscillatory way with the diameter and the illumination wavelength. We show how the conditions of constructive interference can boost the NW absorption up to 50%. The interaction with the metal particles gives rise to variations that are critically dependent on the symmetry of the wire and metal particle modes. These can be engineered to enhance, suppress or even shift the resonant absorption peaks. The importance of the mode symmetry is also confirmed by spatially modifying the modal interaction through a different placement of the particles. As an example, we have shown that with the placement of particles on different facets and controlling the particle wire distance with a spacer oxide, the NW absorption near the band gap energy can be increased by a factor of 5. These findings give new degrees of freedom for engineering light absorption in NWs, bringing new design rules in the planning of opto-electronic devices such as photo-detectors or solar cells.

Acknowledgments

The authors thank Edward S Barnard and Alok Vasudev for assistance with the scanning photocurrent measurements and FDFD simulations. This work was financially supported by the Swiss National Science Foundation through grant numbers 2000021-121758/1 and 129775/1, the SNSF grant for Prospective Researchers number 134484, the NCCR on 'Quantum Science and Technology' and the European Research Council under the UpCon grant.

References

[1] Lu W and Lieber C M 2007 Nanoelectronics from the bottom up *Nat. Mater.* **6** 841–50
[2] Fan Z, Wang D, Chang P-C, Tseng W-Y and Lu J G 2004 ZnO nanowire field-effect transistor and oxygen sensing property *Appl. Phys. Lett.* **85** 5923
[3] Lauhon L J, Gudiksen M S, Wang D and Lieber C M 2002 Epitaxial core-shell and core-multishell nanowire heterostructures *Nature* **420** 57–61
[4] Goto H *et al* 2009 Growth of core-shell InP nanowires for photovoltaic application by selective-area metal organic vapor phase Epitaxy *Appl. Phys. Express* **2** 035004
[5] Tian B *et al* 2007 Coaxial silicon nanowires as solar cells and nanoelectronic power sources *Nature* **449** 885–9
[6] Cao L *et al* 2010 Semiconductor nanowire optical antenna solar absorbers *Nano Lett.* **10** 439–45
[7] Schuller J A and Brongersma M L 2009 General properties of dielectric optical antennas *Opt. Express* **17** 24084–95
[8] Kind H, Yan H, Messer B, Law M and Yang P 2002 Nanowire ultraviolet photodetectors and optical switches *Adv. Mater.* **14** 158–60
[9] Friedler I, Sauvan C, Hugonin J P, Lalanne P, Claudon J and Gérard J M 2009 *Opt. Express* **17** 2095–110
[10] Cao L, Park J-S, Fan P, Clemens B and Brongersma M L 2010 Resonant germanium nanoantenna photodetectors *Nano Lett.* **10** 1229–33

[11] O'Brien S and Pendry J B 2002 Photonic band-gap effects and magnetic activity in dielectric composites *J. Phys.: Condens. Matter* **14** 4035–44
[12] Schuller J A, Zia R, Taubner T and Brongersma M L 2007 Dielectric metamaterials based on electric and magnetic resonances of silicon carbide particles *Phys. Rev. Lett.* **99** 107401
[13] Muskens O L, Diedenhofen S L, van Weert M H M, Borgström M T, Bakkers E P A M and Rivas J G 2008 Epitaxial growth of aligned semiconductor nanowire metamaterials for photonic applications *Adv. Funct. Mater.* **18** 1039–46
[14] Schuller J A, Taubner T and Brongersma M L 2009 Optical antenna thermal emitters *Nat. Photon.* **3** 658–61
[15] Cao L, White J S, Park J-S, Schuller J A, Clemens B M and Brongersma M L 2009 Engineering light absorption in semiconductor nanowire devices *Nat. Mater.* **8** 643–7
[16] Seo K *et al* 2011 Multicolored vertical silicon nanowires *Nano Lett.* **11** 1851–6
[17] Mie G 1908 Beiträge zur Optik trüber Medien, speziell kolloidaler Metallösungen *Ann. Phys.* **330** 377–445
[18] Nobis T, Kaidashev E M, Rahm A, Lorenz M and Grundmann M 2004 Whispering gallery modes in nanosized dielectric resonators with hexagonal cross section *Phys. Rev. Lett.* **93** 103903
[19] Schuller J A, Barnard E S, Cai W, Jun Y C, White J S and Brongersma M L 2010 Plasmonics for extreme light concentration and manipulation *Nat. Mater.* **9** 193–204
[20] Schaadt D M, Feng B and Yu E T 2005 Enhanced semiconductor optical absorption via surface plasmon excitation in metal nanoparticles *Appl. Phys. Lett.* **86** 063106
[21] Westphalen M, Kreibig U, Rostalski J, Lüth H and Meissner D 2000 Metal cluster enhanced organic solar cells *Sol. Energy Mater. Sol. Cells* **61** 97–105
[22] Atwater H A and Polman A 2010 Plasmonics for improved photovoltaic devices *Nat. Mater.* **9** 205–13
[23] Okamoto K, Vyawahare S and Scherer A 2006 Surface-plasmon enhanced bright emission from CdSe quantum-dot nanocrystals *J. Opt. Soc. Am.* B **23** 1674–8
[24] Nie S and Emory S R 1997 Probing single molecules and single nanoparticles by surface-enhanced Raman scattering *Science* **275** 1102–6
[25] Hyun J K and Lauhon L J 2011 Spatially resolved plasmonically enhanced photocurrent from Au nanoparticles on a Si nanowire *Nano Lett.* **11** 2731–4
[26] Dick K A 2008 A review of nanowire growth promoted by alloys and non-alloying elements with emphasis on Au-assisted III–V nanowires *Prog. Cryst. Growth Char. Mater.* **54** 138–73
[27] Schmidt V, Wittemann J V, Senz S and Gösele U 2009 Silicon nanowires: a review on aspects of their growth and their electrical properties *Adv. Mater.* **21** 2681–702
[28] Krogstrup P, Curiotto S, Johnson E, Aagesen M, Nygård J and Chatain D 2011 Impact of the liquid phase shape on the structure of III–V nanowires *Phys. Rev. Lett.* **106** 125505
[29] Fontcuberta i Morral A, Colombo C, Abstreiter G, Arbiol J and Morante J R 2008 Nucleation mechanism of gallium-assisted molecular beam epitaxy growth of gallium arsenide nanowires *Appl. Phys. Lett.* **92** 063112
[30] Colombo C, Spirkoska D, Frimmer M, Abstreiter G and Fontcuberta i Morral A 2008 Ga-assisted catalyst-free growth mechanism of GaAs nanowires by molecular beam epitaxy *Phys. Rev.* B **77** 155326
[31] Ross F M, Tersoff J and Reuter M C 2005 Sawtooth faceting in silicon nanowires *Phys. Rev. Lett.* **95** 146104
[32] Klauk H 2008 Device physics: nanowires' display of potential *Nature* **451** 533–4
[33] Nikoobakht B 2007 Toward industrial-scale fabrication of nanowire-based devices *Chem. Mater.* **19** 5279–84
[34] Chan C K *et al* 2008 High-performance lithium battery anodes using silicon nanowires *Nat. Nano* **3** 31–5
[35] Atwater H A, Lewis N S and Kayes B M 2005 Comparison of the device physics principles of planar and radial p–n junction nanorod solar cells *J. Appl. Phys.* **97** 114302
[36] Fontcuberta i Morral A, Spirkoska D, Arbiol J, Heigoldt M, Morante J R and Abstreiter G 2008 Prismatic quantum heterostructures synthesized on molecular-beam epitaxy GaAs nanowires *Small* **4** 899–903
[37] Demichel O, Heiss M, Bleuse J, Mariette H and Fontcuberta i Morral A 2010 Impact of surfaces on the optical properties of GaAs nanowires *Appl. Phys. Lett.* **97** 201907

[38] Colombo C, Heiß M, Grätzel M and Fontcuberta i Morral A 2009 Gallium arsenide p–i–n radial structures for photovoltaic applications *Appl. Phys. Lett.* **94** 173108

[39] Fontcuberta i Morral A, Spirkoska D, Arbiol J, Heigoldt M, Morante J R and Abstreiter G 2008 Prismatic quantum heterostructures synthesized on molecular-beam epitaxy GaAs nanowires *Small* **4** 899–903

[40] Arbiol J *et al* 2009 Long range epitaxial growth of prismatic heterostructures on the facets of catalyst-free GaAs nanowires *J. Mater. Chem.* **19** 840

[41] Pala R A, White J, Barnard E, Liu J and Brongersma M L 2009 Design of plasmonic thin-film solar cells with broadband absorption enhancements *Adv. Mater.* **21** 3504–9

[42] Cao L, Park J-S, Fan P, Clemens B and Brongersma M L 2010 Resonant germanium nanoantenna photodetectors *Nano Lett.* **10** 1229–33

[43] Veronis G and Fan S 2007 Overview of simulation techniques for plasmonic devices *Surface Plasmon Nanophotonics* ed M L Brongersma and P G Kik (Dordrecht: Springer) pp 169–82

[44] Barnard E S, White J S, Chandran A and Brongersma M L 2008 Spectral properties of plasmonic resonator antennas *Opt. Express* **16** 16529–37